

Cite this: DOI: 00.0000/xxxxxxxxxx

Ultrafast energy transfer between lipid-linked chromophores and plant Light-Harvesting Complex II[†]

Ashley M. Hancock,^{a,b‡} Minjung Son,^{c,d‡} Muath Nairat,^c Tiejun Wei,^f Lars J. C. Jeuken,^{b,e} Christopher D. P. Duffy,^f Gabriela S. Schlau-Cohen^{*c} and Peter G. Adams^{*a,b}

Received Date

Accepted Date

DOI: 00.0000/xxxxxxxxxx

The Light-Harvesting Complexes (LHCs) found in plants are membrane protein complexes which perform solar energy absorption and subsequent transfers of electronic excitation energy with high efficiency. We previously demonstrated a bio-hybrid system where plant Light-Harvesting Complex II (LHCII) proteins were assembled into lipid membrane vesicles together with lipid-linked Texas Red (TR) chromophores which enhance the spectral range of the system. In the current study, we use a combination of spectroscopy experiments and computational simulations to explain the interactions between TR and LHCII in nanodiscs. We find that TR-to-LHCII energy transfer has >60% efficiency and results in an enhancement of LHCII fluorescence is significantly greater in the nanodiscs system as compared to our previous work using vesicles, 255% versus 120%. Ultrafast transient absorption spectroscopy revealed two distinct time constants of 3.7 and 128 ps for TR-to-LHCII energy transfer, which are likely due to two distinct interactions between TR and LHCII. Molecular Dynamics simulations of the lipid and protein motion and theoretical calculations of excitation energy transfer provide important insight into the structural context of TR-LHCII interactions. It appears that one population of TR-lipids is freely diffusing in the membrane and the other is closely associated with the protein (estimated TR-LHCII distances of ~3.5 nm and ~1 nm, respectively). Overall, this nanodisc based hybrid system has significance as an idealized platform to test the photophysical interactions between extrinsic chromophores and membrane proteins relevant to both natural LHCs and artificial photosynthesis.

1 Introduction

Light-harvesting protein complexes (LHCs) are crucial for effectively absorbing solar energy in the first stages of photosynthesis, acting like a satellite dish, they direct and concentrate energy towards reaction centre protein complexes where the photochemical trapping of energy takes place.¹ A variety of LHCs exist across biology, but the majority are membrane proteins which have a specific 3-D polypeptide structure coordinating a network

of pigments.^{2–4} Light-harvesting complex II (LHCII) is the major component of the peripheral antenna for the Photosystem II supercomplex⁵ in higher plants and green algae, it contains a pigment network of 8 chlorophyll (Chl) *a*, 6 Chl *b* and 4 xanthophyll carotenoids.^{6,7} The pigments held within the protein scaffold form a dense array with inter-pigment distances as short at 0.97 nm, which enables the rapid and efficient transfer of excitation energy between pigments.^{8,9} Excitation energy transfer between pigments at distances above ~1 nm can be accurately described with Förster theory for resonance energy transfer (FRET), as the hopping of localized excited states from one pigment to the next.³ For tightly-coupled pigments at distances under ~1 nm, excitation energy may be delocalized across multiple pigments and so-called "coherent" transfer of energy may be described by Redfield theory.¹⁰ There has been great effort to understand the pathways for efficient transfer of excitation energy within and between LHCs and reaction centres. There is also ongoing debate over the identity of "photoprotective" pathways which exist within LHCII for the deliberate dissipation of energy under high-light conditions.^{5,11–14} Questions remain over the details of the underlying photophysical processes, including which specific pig-

^a School of Physics and Astronomy, University of Leeds, Leeds LS2 9JT, UK. E-mail: p.g.adams@leeds.ac.uk

^b Astbury Centre for Structural Molecular Biology, University of Leeds, Leeds LS2 9JT, UK.

^c Department of Chemistry, Massachusetts Institute of Technology, 77 Massachusetts Ave, Cambridge, MA 02139, USA. E-mail: gscc@mit.edu

^d Current Address: Department of Chemistry, University of Wisconsin–Madison, 1101 University Ave, Madison, WI 53706, USA.

^e Faculty of Biological Sciences, University of Leeds, Leeds LS2 9JT, UK.

^f School of Biological and Chemical Sciences, Queen Mary University of London, Mile End Road, London E1 4NS, UK.

† Electronic Supplementary Information (ESI) available: [details of any supplementary information available should be included here]. See DOI: 00.0000/00000000.

‡ These authors contributed equally to this work.

ments are involved, their excitonic character and the timescales involved.^{15–17} It is challenging to resolve the molecular details of proteins within their natural environment due to the complexity and dynamic nature of cells.¹⁸ Therefore, photosynthetic membrane proteins have been extensively studied in an isolated form, which allows the function and processes associated with specific proteins to be identified. Detergents can provide stable structures for isolating membrane proteins, and studies on LHCII isolated within detergent micelles have been highly revealing, showing the electronic structure of specific carotenoids, Chl-Chl interactions,^{19–21} how proteins self-associate,²² and the switching between different possible emissive states.²³ However, detergents can often disrupt the structure of membrane proteins and therefore the ensued dynamics poorly mimics the natural biomembrane environment.²⁴ In order to understand the physiologically relevant properties of LHCII, studies can be performed with the protein incorporated into a more native environment that includes a lipid bilayer.

Model membranes are an experimental system where membrane proteins are reconstituted into lipid bilayers at a defined protein-to-lipid ratio, which provides a native-like local lipid environment. The most common type of model membranes studied are spherical vesicles typically hundreds of nanometers in diameter, termed “proteoliposomes”. Proteoliposomes provide an appropriate 2-D confined expanse for membrane proteins, but can have uncertainties including the level of membrane curvature and the possibility of multiple (up/down) protein orientations within a single membrane.²⁵ Protein-protein interactions can be studied within proteoliposomes, however, such interactions can sometimes cause undesirable effects, e.g., in-membrane protein aggregation can cause changes to protein structure which may or may not be relevant to those found in nature.^{26–31} One alternative to proteoliposomes is to utilize disc-shaped model membranes, termed “lipid nanodiscs”, which are much smaller than liposomes, with a defined diameter determined by the particular “belting protein” (BP) used. With these dimensions, typically only one LHCII is incorporated per nanodisc, limiting the potential for protein-protein interactions to occur. Thus, nanodiscs could be particularly valuable when studying plant LHCII where protein-protein and protein-lipid interactions have major effects on its fluorescence and energy dissipation pathways.^{24,30,32–35} Therefore, nanodiscs can be employed to study single isolated membrane proteins (as with detergent micelles) but allow the additional benefit of the lipid bilayer environment (as with proteoliposomes), providing the desired advantages of both systems.

Synthetic chromophores can be interfaced with LHCs in order to provide additional pathways to inject excitation energy, where the extra chromophores are selected for their complementary spectral range or other photophysical properties of interest. Several studies have demonstrated successful energy transfer that resulted in an enhancement of the absorption range of the combined LHC-chromophore system as compared to native LHC. In these cases, energy transfer between synthetic and natural chromophores is non-radiative, analogous to transfer between natural chromophores in LHCs and can be generally described by simple FRET relationships. Typically, an approach of genetic manip-

ulation or specific linker chemistry has been employed to covalently attach the chromophore to the protein.^{36–43} In the best case, a hybrid chromophore-LHC system was reported with an effective absorption efficiency of up to 7 times relative to the unmodified LHC in the wavelength range where the protein’s absorption is normally minimal.³⁹ The efficiency of chromophore-to-protein energy transfer has been shown to surpass 85% for some hybrid systems, equating to an energy transfer timescale of femto-to-picoseconds, i.e., on the same order as the timescale of inter-pigment energy transfer in natural LHCs.³⁸ The constraint of a covalent attachment strategy is that it results in a fixed system typically with one chromophore attached at a specific position to the LHC.

Recently, we presented a flexible, non-covalent approach for interfacing synthetic chromophores to LHCs: a small, organic, lipid-linked “Texas Red” (TR) chromophore, which absorbs strongly in the region of minimal natural LHCII absorption, was co-assembled with plant LHCII into model lipid membranes.⁴⁴ This approach exploited the spontaneous self-assembly of lipids to drive the system’s formation and allowed a higher level of modularity than would be possible with chemical cross-linking or genetic modification. Specifically, the density of additional chromophores within the membrane system could be varied by simply changing the ratio of TR-lipids to normal lipids in the starting lipid mixture. Energy transfer was demonstrated from TR to LHCII with an efficiency up to 95%, and up to a three-fold enhancement of the fluorescence intensity of LHCII, when illuminating in the region of minimum natural absorption.⁴⁴ The lipid-linked nature of TR allows it to be located within the lipid bilayer at a variable distance away from the protein, often 1–10 nm, comparable to the typical protein-protein distances found within natural light-harvesting membranes. Therefore, we note that model lipid membranes containing extrinsic chromophores such as these, could be a useful platform to probe picosecond-timescale photophysical processes that have relevance to inter-LHC excitation energy transfer. Our previous investigation of TR and LHCII⁴⁴ used proteoliposomes so that the interactions between many TR molecules and LHCII proteins could be observed; now, we propose that lipid nanodiscs could provide an elegant platform where interactions between TR and singular LHCII proteins can be observed within a confined membrane area. In the current study, we: (i) assess the level of fluorescence enhancement achieved for LHCII/TR when using lipid nanodiscs with steady-state spectroscopy, (ii) measure the timescale of TR-to-LHCII energy transfer with ultrafast time-resolved spectroscopies, and (iii) generate a structural simulation of the system and perform theoretical calculations to consider the molecular basis for these interactions.

2 Results

2.1 Formation of model membrane samples

Four components were required for our nanodisc samples: (i) the “belting protein” which forms the enclosure of the disc and constrains its size, (ii) the LHCII membrane protein which is to be incorporated, (iii) the TR-lipid doped into the lipid bilayer at a

low molar fraction, (iv) the bulk lipid which forms the majority of the lipid bilayer. Our nanodiscs have the capacity to incorporate single LHCII proteins into a lipid bilayer at close proximity to multiple TR molecules, as shown in Fig. 1A. We chose a particular belting protein that generates relatively large discs (ApoE422K), expected to have diameters of 25-30 nm. This was designed to provide a sufficient area around the LHCII to allow free lipid diffusion within the lipid bilayer annulus: there would be an average distance of 7.5-10 nm from the outer surface of a centrally-located LHCII to the disc edge.⁴⁵ These dimensions allowed a range of donor-acceptor separations to be sampled as the protein and lipids diffuse laterally within the nanodisc, therefore, TR-LHCII separation distances both above and below the expected Förster radius (approx. 7 nm) can be achieved. The LHC used for all experiments was trimeric LHCII protein biochemically purified from spinach using the detergent n-Dodecyl- α -D-Maltopyranoside (α -DDM), as previously described (see ESI 2.1).¹¹ The ApoE422K belting protein was expressed and purified as previously described (see ESI 2.2).²⁴ The TR-lipid is commercially available for use in probing lipid bilayers and was used as purchased.⁴⁴ For all samples, the lipid mixture used was soy asolectin which has been previously shown to provide a stable membrane environment for plant light-harvesting proteins reconstituted into nanodiscs.²⁴

Three samples were prepared after several rounds of optimization: (i) TR-LHCII nanodiscs as the main test sample; (ii) LHCII nanodiscs as the acceptor-only control sample; (iii) TR liposomes as the donor-only control samples. Note that nanodiscs were not required in the absence of LHCII, so, for sample (iii) liposomes were used for simplicity formed by following a typical sonication method.¹¹ LHCII nanodiscs were assembled from a starting mixture of a lipid:BP:LHCII ratio of 3000:12.5:1, selected so that on average 6-7 belting proteins will associate to form a 25-30 nm disc with ~1500 lipids and 0 or 1 LHCII trimer. For samples containing TR this was included in the starting lipid mixture at a molar ratio of 1:75 relative to total lipids (1.3% mol/mol). A standard nanodisc assembly procedure was followed,²⁴ starting with a detergent-solubilized lipid-LHCII-BP mixture, and then removing the detergent with Biobeads which induces the self-assembly of membranes. Any LHCII or lipids which were not incorporated into the disc assembly were removed by nickel-NTA affinity chromatography (the belting protein sub-units are histidine-tagged) and the elution profile data suggested that the formation process was successful for all samples (see ESI 2.3). Particle characterisation measurements were performed on nanodisc samples to determine the distribution of the disc sizes and to rule out the presence of any large protein aggregates. Transmission Electron Microscopy (TEM) analysis gave an average nanodisc diameter of 21 ± 7 nm (S.D.), in agreement with dynamic light scattering (DLS) measurements (see ESI 2.4). Importantly, neither TEM or DLS indicated the presence of any large aggregates of proteins or lipids and suggested that the vast majority of particles in the final preparation were individual nanodiscs. Therefore, the predominant TR-LHCII interactions were considered to be between multiple TR moieties and single LHCII proteins reconstituted into discs.

2.2 Steady-state spectroscopy

To determine the concentrations of LHCII and TR achieved within the membrane samples and to assess any spectral shifts, steady-state absorption spectroscopy was performed. The absorption spectra of all three samples are shown in Fig. 1 (solid lines) and the shape and position of the peaks representing LHCII and TR can be compared. The absorption peaks representing LHCII at 400-500 nm and 630-700 nm are identical both in the presence and absence of TR suggesting that TR has no direct effect on the pigment structure within LHCII (blue vs green solid lines or spectra in Fig. 1B). These peaks are very similar to the absorption spectrum for isolated LHCII in detergent micelles (see ESI 2.5). Therefore, nanodiscs appear to maintain the structure and pigment composition of reconstituted LHCII while providing a more native-like lipid environment than detergent micelles. The TR peak at ~590 nm has the expected shape and position in its samples, whether it is within nanodiscs or liposomes. Analysis of the sample absorption spectra allowed the absolute concentration of each component to be calculated using known absorption coefficients after spectral decomposition to isolate the signal from each component (see ESI 2.6/2.7). The TR-LHCII nanodisc sample had an estimated lipid:TR:LHCII ratio of 2870:38.3:1 (with the assumption that the ratio of TR-lipid to normal lipids is not altered during the assembly process), confirming that sample preparation was successful.

TR-to-LHCII energy transfer was assessed via steady-state fluorescence spectroscopy with selective excitation of TR at 540 nm (where LHCII has minimal absorption). As shown in Fig. 1C, the fluorescence intensity of TR was significantly reduced in the membranes which also included LHCII compared to those without (solid vs dashed pink line). This quenching of the emission from TR (the energy donor) was quantified as 38%, therefore, the efficiency of resonance energy transfer from TR-to-LHCII is estimated as 62% according to simple Förster theory interpretation (see ESI 2.8).⁴⁴ This value for transfer efficiency correlates to independent measurements using a comparison between LHCII fluorescence excitation spectra and "absorptance" (1 - transmission) spectra which suggested an efficiency ~65% (see ESI 2.9). This estimated efficiency is likely to be an underestimate for TR-to-LHCII transfers due to a sub-population of TR in nanodiscs not interacting with LHCII (see section 3.2 for further discussion).

LHCII fluorescence can also be assessed to show the direct effect of TR on LHCII's photophysical properties. Probing isolated LHCII with 540 nm excitation leads to a minimal level of fluorescence, whereas, in the combined system an enhancement of LHCII fluorescence would be expected if additional energy is transferred from TR donors to LHCII acceptors. Indeed, the fluorescence intensity of LHCII in nanodiscs was increased by 255% (see Table 1 in ESI) the presence of TR when excited at 540 nm (solid vs dashed green line in Fig 1C) relative to LHCII isolated in detergent.

2.3 Time-resolved fluorescence

In order to determine the timescale of FRET from TR to LHCII, time-resolved fluorescence spectra (TRFS) of all three samples were measured by selectively exciting the TR donor and simul-

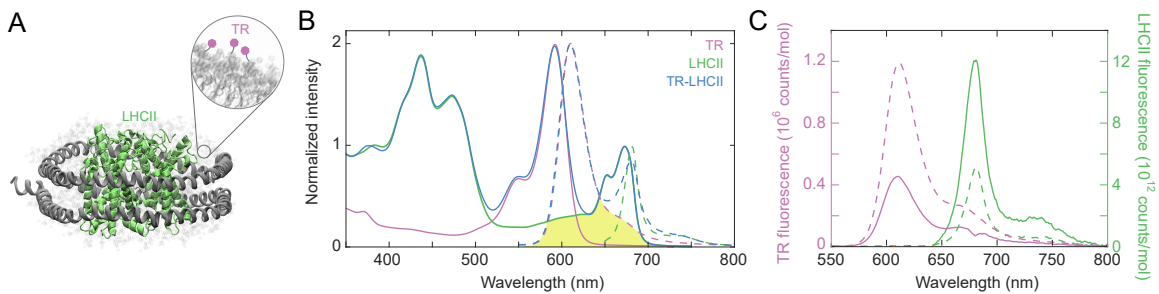


Fig. 1 (A) Cartoon illustration of the nanodisc co-reconstituting TR-lipid and LHCII. TR-lipid is shown in light gray with TR molecules in purple (inset), LHCII is shown in green, and the belting protein (ApoE422K) is shown in dark gray. (B) Steady-state absorption (solid lines) and fluorescence emission spectra (dashed lines) of the TR liposomes (pink), the TR-LHCII nanodiscs (blue), and the LHCII nanodiscs (green) samples. Spectra are normalized to an intensity of 1 at either the Chl *a* peak (~ 680 nm) or the TR peak (~ 600 nm), for clarity. The spectral overlap between the TR emission peak (energy donor) and the LHCII absorption peak (energy acceptor) is shown as the yellow shaded area. The excitation wavelengths used in fluorescence measurements are 540 nm (TR, TR-LHCII) and 630 nm (LHCII). (C) Steady-state fluorescence emission spectra acquired with excitation at 540 nm (2 nm bandwidth), focusing on the peak due to TR emission (in pink) or LHCII emission (in green). The control samples containing only one component are shown as a dashed line and the main test sample containing both components are shown as solid lines. For clarity, the spectrum from the TR-LHCII sample was decomposed into its component TR and LHCII peaks (see ESI 2.6). For comparison, all spectra are shown as the “relative emission per mole”, where the TR peak is divided by the calculated molar TR concentration and the LHCII peak is divided by the calculated molar LHCII concentration (see ESI 2.7).

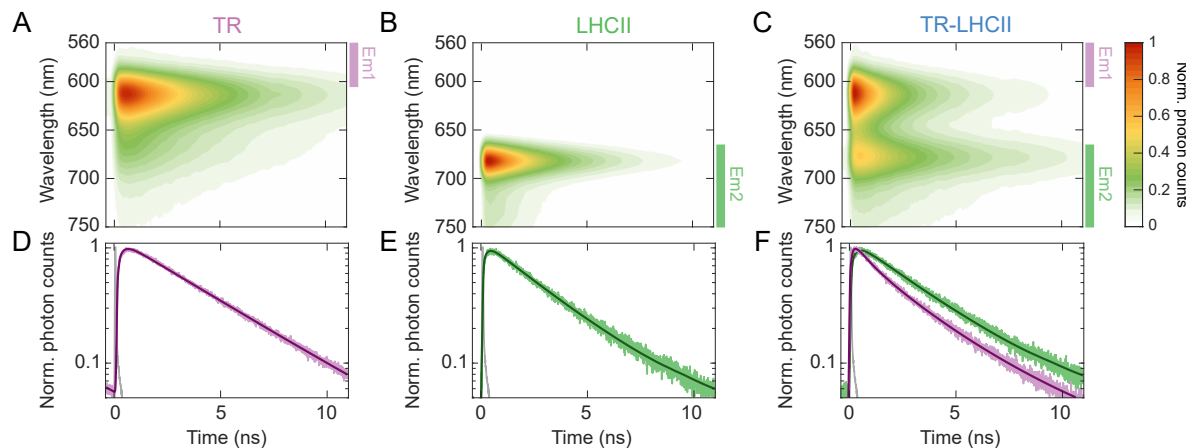


Fig. 2 Normalized TRFS of TR liposomes (A), LHCII nanodiscs (B), and TR-LHCII nanodiscs (C). (D)–(F) Fitted decay traces of the TRFS shown in (A)–(C). The wavelength ranges over which the fluorescence signal was integrated are labeled in (A)–(C) with colored bars (Excitation at 550 nm. Em1: 560–600 nm, Em2: >665 nm.; see ESI 2.11). The instrument response function (IRF) is shown in gray in (D)–(F).

taneously detecting the fluorescence dynamics across the entire emission range of each sample (Fig. 2 and ESI 2.10). The TRFS of TR liposome (see Fig. 2A) and LHCII nanodisc (Fig. 2B) exhibit emission maxima at 614 nm (TR) and 682 nm (LHCII), respectively, accompanied by vibronic bands at 673 nm (TR) and 735 nm (LHCII), in accordance with their steady-state fluorescence spectra. The fluorescence decay kinetics do not show dependence on the emission wavelength for either sample (see ESI 2.11). The fluorescence decay of TR liposome was fitted to a monoexponential decay with a lifetime of 3.94 ± 0.20 ns (Fig. 2D), in agreement with the value reported in the literature of ~ 4 ns for isolated TR chromophores.⁴⁶ The LHCII nanodisc showed a biexponential decay profile, resulting in an average fluorescence lifetime ($\langle \tau_{\text{fl}} \rangle$) of 2.68 ± 0.06 ns (Fig. 2E) which represents a moderate degree of quenching ($\sim 30\%$) as compared to the lifetime reported for LHCII isolated in detergent micelles of ~ 4 ns.^{11,26,47} Such quenching of LHCII fluorescence in nanodiscs has been re-

ported previously, and attributed to conformational changes in LHCII induced by the local membrane environment.^{24,34,48}

The TRFS of the TR-LHCII nanodisc (Fig. 2C) appears as the combination of those of TR and LHCII, with emission maxima at 614 nm and 677 nm. The first band originates almost exclusively from TR fluorescence, and the second band contains mixed contributions from both the (0-1) vibronic band of TR fluorescence and the (0-0) band of LHCII fluorescence. Unlike for the TR liposome or LHCII nanodisc, the fluorescence decay profile of the TR-LHCII nanodisc shows dependence on the emission wavelength, due to the presence of both TR and LHCII. We monitored two emission ranges, labeled Em1 and Em2 in Fig. 2, which correspond to the two bands mentioned above. In the emission range (Em1), which reports the decay of the TR fluorescence, we observe a 68% decrease in the $\langle \tau_{\text{fl}} \rangle$ of the TR-LHCII nanodiscs compared to that of the TR liposome, from 3.94 ± 0.20 ns to 1.28 ± 0.03 ns (Table 1). This drastic reduction in the fluorescence lifetime

Table 1 Fit parameters from time-resolved fluorescence measurements^a

	A_1 (%)	τ_1 (ns)	A_2 (%)	τ_2 (ns)	$\langle \tau_{\text{fl}} \rangle$ (ns)
TR (Em1)	—	—	100	3.94 ± 0.20	3.94 ± 0.20
LHCII (Em2)	10.2 ± 0.4	0.33 ± 0.04	89.8 ± 0.4	2.95 ± 0.07	2.68 ± 0.06
TR-LHCII (Em1)	58.8 ± 0.4	0.32 ± 0.02	41.2 ± 0.4	2.64 ± 0.06	1.28 ± 0.03
TR-LHCII (Em2)	66.4 ± 0.6	2.60 ± 0.20	33.6 ± 0.6	3.92 ± 0.08	3.17 ± 0.13

^a A: percent amplitude, τ : time constant, $\langle \tau_{\text{fl}} \rangle$: amplitude-weighted average fluorescence lifetime ($\langle \tau_{\text{fl}} \rangle = A_1 \tau_1 / 100 + A_2 \tau_2 / 100$). The errors shown after the +/- symbol are the 95% confidence intervals of the fit.

of TR is due to excitation energy transfer to LHCII. From the percent decrease in $\langle \tau_{\text{fl}} \rangle$ we determine that the FRET efficiency is 68%, in good agreement with the 62% efficiency calculated from the analysis of the steady-state fluorescence presented in section 2.2. The fluorescence decay in the red emission range (Em2) is best fitted to a biexponential decay profile, resulting in a longer $\langle \tau_{\text{fl}} \rangle$ of 3.17 ± 0.13 ns compared to that of LHCII without the TR donor. This apparent lengthening of $\langle \tau_{\text{fl}} \rangle$ is attributed to the aforementioned convolution of the LHCII fluorescence with the (0-1) vibronic band of TR, which has a longer lifetime as well as a higher fluorescence quantum yield than those of LHCII, and thus skew the dynamics toward a slower fluorescence decay. We do not observe any rise component that is slower than the instrument response function (IRF) in this range, which suggests that the FRET timescale is shorter than the time resolution of the fluorescence measurement (50 ps).

2.4 Transient absorption

The ultrafast timescale of energy transfer from TR to LHCII was measured with femtosecond transient absorption (TA) spectroscopy. The pump laser spectrum was tuned to preferentially excite the absorption band of the TR donor from 500 to 600 nm. A broadband probe pulse spanning both the TR and LHCII transitions was employed (see ESI 2.12). Due to the weak absorption of LHCII in the pump wavelength range that partly overlaps with TR absorption, assigned to higher vibronic levels of the Q_x and Q_y states of the Chls,^{49,50} a small percentage (~20%) of the excited state measured is due to direct absorption by the Chls. These higher vibronic states undergo rapid internal conversion within the vibronic manifold on a ~200 fs timescale to the lowest vibronic level of Q_y .^{51–53} To benchmark the excited state dynamics of the TR donor and the LHCII acceptor in the absence of their FRET partner, we measured the TA of TR liposome and LHCII nanodisc. The TA map of TR liposome (Fig. 3A/B) shows ground-state bleach (GSB) and stimulated emission (SE) with a main peak at 593 nm and a minor peak at ~600 nm, in accordance with the vibronic band structure seen in the steady-state absorption and fluorescence spectra. Both peaks exhibit a mono-exponential decay with a time constant of 1.17 ± 0.02 ns (see ESI 2.13). The TA map of LHCII nanodisc (Fig. 3C/D) shows an intense band peaking at ~675 nm, which is the GSB/SE of the Chl a Q_y state. The TA signal at shorter wavelengths (< 650 nm) is very weak due to the low oscillator strength of the higher vibronic states as well as overlapping contributions from the negative GSB/SE and positive excited state absorption (ESA).^{54,55} Throughout this section, the raw TA data for each sample is processed by a "global analysis" procedure which allows us to assign

time constants to specific processes over defined wavelength regions associated with LHCII and Texas Red signal. The LHCII GSB/SE decay was adequately fit with a single time constant of 903 ± 8 ps (see ESI 2.13). For both TR and LHCII, the fitted time constant from the TA is shorter than the lifetime extracted from the TRFS (Table 1) because of the limited temporal window of our TA measurement (0–700 ps). The TA map of the TR-LHCII nanodisc (Fig. 3E/F) exhibits spectral features of both TR and LHCII, *i.e.*, the GSB/SE from TR centered at 593 nm and that from LHCII Chl a centered at ~665 nm. Comparison of the decay of the donor TR peak with and without the acceptor LHCII demonstrates significant acceleration of the TR decay in the presence of LHCII (Fig. 3 G). Global analysis reveals that TR excited states have a much faster biexponential decay with time constants of 3.7 ± 0.1 ps and 128 ± 1 ps in the presence of LHCII (compared to the 1.17 ns time constant in the absence of LHCII). In addition, we observe a rise of the LHCII GSB/SE band on a similar timescale (Fig. 3H). These results clearly indicate the presence of energy transfer from TR to LHCII on a picosecond timescale. The transient in the 650–680 nm wavelength range exhibits convoluted dynamics originating from multiple overlapping contributions. In addition to the LHCII SE populated through energy transfer from TR, two other contributions, SE from the (0-1) vibronic band of TR and SE from direct population of higher vibronic levels of LHCII followed by downhill internal conversion, appear in this region and partially interfere with the signature for energy transfer. While the correlated decay of TR and rise of LHCII populations provide qualitative evidence for the energy transfer from TR to LHCII, extracting quantitative timescales is challenging. Global analysis of the TA data attempts to disentangle the multiple competing processes and assigns timescales to each step. Global fits of the TA data at selective wavelengths for LHCII and TR components in TR-LHCII nanodiscs are shown in Fig. 4A. The best description of the energy transfer dynamics in TR-LHCII nanodiscs was obtained using a three-level sequential model illustrated in Fig. 4B. The extracted evolution-associated difference spectra (EADS) with the respective time constants are shown in Fig. 4C. The first two EADS, which are associated with time constants of 3.7 and 128 ps (EADS1 and EADS2, respectively, in Fig. 4C), represent a bi-exponential decay of the TR peak at 593 nm. Furthermore, these EADS show a growth in the TA signal at longer wavelengths with predominantly LHCII contribution (> 650 nm), as demonstrated by the positive sign of decay-associated difference spectra (DADS) shown in ESI 2.13 Fig. S13, in DADS2 and to a lesser extent in DADS1. The TR liposome DADS (ESI Fig. S12) lacks this positive signature seen in TR-LHCII nanodiscs at wavelengths longer than 650 nm due to the occurrence of energy transfer in the lat-

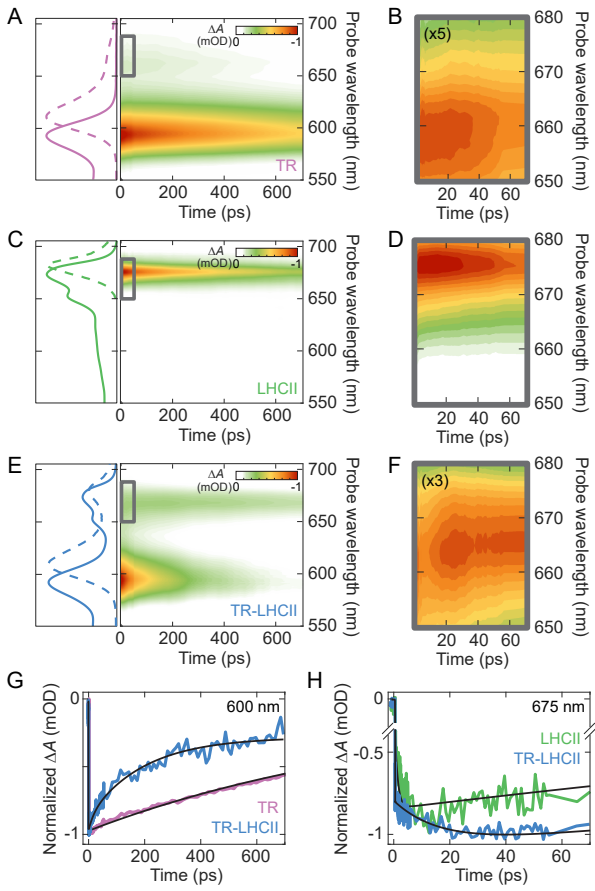


Fig. 3 Normalized TA maps of TR liposome (A, B), LHCII nanodisc (C, D), and TR-LHCII nanodisc (E, F). Steady-state absorption (solid lines) and fluorescence (dashed lines) spectra of each sample are shown on the left. (B), (D), (F) are magnifications of the region of the TA maps where the Chl Q_y GSB/SE range is apparent for the initial 70 ps (gray boxes in (A), (C), (E)). The color-scale in the maps in (B) and (F) are multiplied by a factor of 5 and 3, respectively, for clarity. (G) Normalized fitted time traces at 600 nm to demonstrate the difference in TR excited state decay. (H) Normalized fitted time traces at 675 nm demonstrating the rise in the population of LHCII excited states (initial 70 ps). The black lines in (G) and (H) show the fits discussed in the text.

ter. Thus, we assign these two components to the timescales of energy transfer from TR to LHCII. The biexponential decay kinetics observed suggests that the energy transfer is heterogeneous in its nature, as may be expected from a distribution of donor-acceptor distances within the nanodisc due to a large range of positions that TR-lipids can locate within the expanse of lipid bilayer. We assign the 3.7 ps time constant to a fast energy transfer step with a subpopulation of TR that is embedded in close proximity to LHCII within the nanodisc, and the 128 ps time constant to another subpopulation that is located further away from the LHCII acceptor. The final, long-lived EADS represents the decay processes which are significantly slower than the time window of the TA measurements (EADS3 in Fig. 4C). It is likely that this EADS represents the combination of the nanosecond decay of LHCII and the nanosecond decay of a sub-population of TR located within lipid nanodiscs that do not interact with LHCII. The nominal time constant of 1.03 ns appears shorter than the fluo-

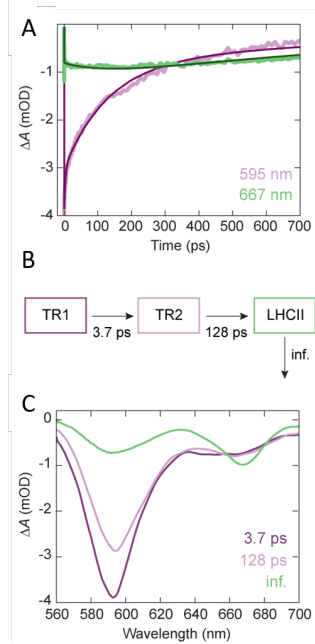


Fig. 4 (A) Global fit of the TA decay traces at 595 nm (purple) and 667 nm (green). Note the similarity in the traces to the raw data displayed for TR-LHCII nanodiscs in Fig. 3G/H. (B) Kinetic model of the dynamics observed in TR-LHCII nanodisc with the associated time constants obtained from global analysis of the TA data. (C) EADS of the three components shown in (B): EADS1 (3.7 ps), EADS2 (128 ps), EADS3 (inf.).

rescence lifetime of LHCII due to the limited temporal window of our TA measurement as mentioned earlier.

2.5 Molecular Dynamics simulations and energy transfer rates

Next, we wished to explain the structural context for the FRET timescales observed. The simplest possible arrangement would be a single LHCII trimer embedded centrally within the lipid nanodiscs, as shown in the cartoon in Fig. 5A. Of course, this cartoon is woefully imprecise and does not properly consider structural clashes and other interactions and fails to consider any protein/lipid dynamics within the system. In order to get a more accurate picture of the interactions and timescales occurring within TR-LHCII nanodiscs we performed a set of short Molecular Dynamics (MD) simulations. A bilayer membrane comprised of 500 1,2-dioleoyl-sn-glycero-3-phosphocholine (DOPC) lipids was generated with both width and length of 125 Å. An LHCII monomer, structure adopted from Protein Data Bank (PDB) 1rwt,⁵⁶ was inserted into the bilayer⁵⁷ with steric clashed lipids carefully removed (see ESI 2.14 for more detailed description). Note, a monomer was chosen for computational simplicity as in other previous MD simulations of LHCII.¹³ In accordance with the experimental concentration, five TR-tagged lipids were placed randomly in the membrane. The final system is shown in Fig. 5B. All five were positioned at what, in the native membrane, would be the stromal side of the protein, although both orientations are likely sampled in the nanodisc. The system was first equilibrated over 20 ns before five independent simulations were per-

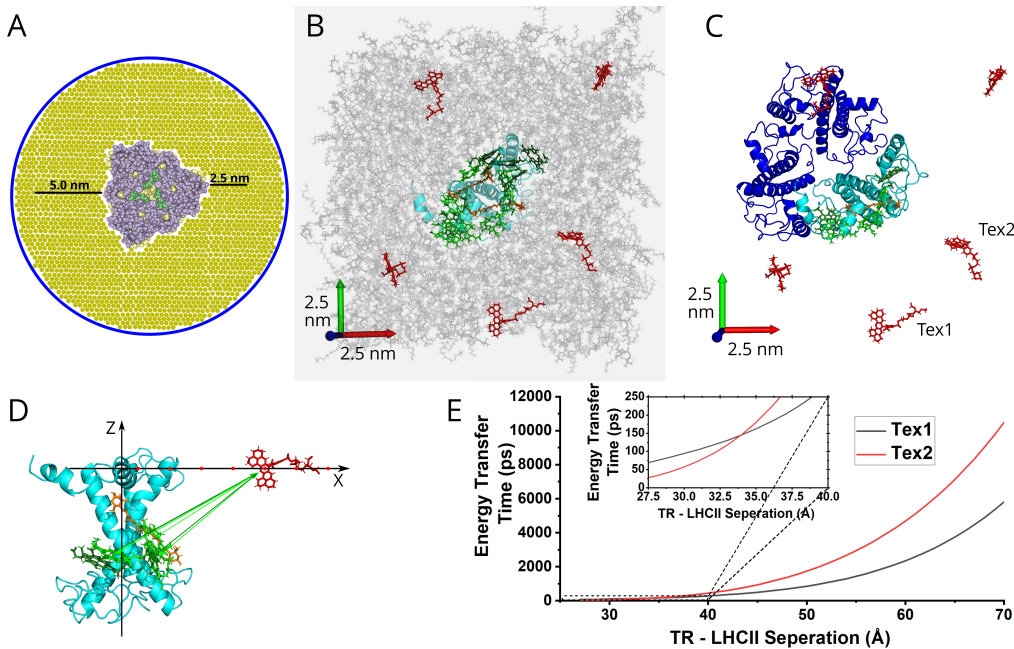


Fig. 5 (A) Cartoon of our lipid nanodisc system showing an LHCII trimer (grey), surrounded by lipids (yellow), with the approximate boundary region of the nanodisc is denoted in blue (top down view). This cartoon is approximately to scale. Not all lipids displayed for clarity. (B) Molecular Dynamics model of the TR-LHCII-lipid system (top down view) at the start of the simulation, $t = 0$. Shown are approximately 500 DOPC lipids (grey), 5 Texas Red (red), one LHCII monomer (polypeptide in cyan, Chls in green, carotenoids in orange). Only the most relevant pigments are displayed for clarity. 10541 TIP3P water molecules are present in the simulation but are not displayed. (C) Representation of the system from (B), except overlaid with the position of a possible LHCII trimer. The two TR molecules of interest which were chosen for further analysis are noted (Tex1 and Tex2). Lipids are not displayed for clarity. (D) Side-on view of the structural model demonstrating the simulated changing lateral position of the Texas Red molecule relative to LHCII incorporated into the lipid bilayer. The structural coordinates of the protein were fixed according to the MD model and the location of Tex1 (or Tex 2) was varied by translocating it along the vector shown (black line with red dots). At each separation distance and relative orientation, the resonance couplings (green arrows) were then calculated according to the point dipole approximation (see ESI 2.17). (E) Graph showing the TR-to-Chl transfer times (k^{-1}) as a function of the overall TR-LHCII separations varied as shown in (D), computed from the resonance couplings and the spectral overlaps for all likely transitions, following Förster theory as detailed in ESI 2.17. The inset graph magnifies low-distance regime for increased clarity.

formed of 60 ns duration each. The resulting trajectories were analyzed in order to reveal the motion of the protein, lipids and TR (see **SUPPLEMENTARY MOVIE**). The calculated diffusion constant for the non-tagged lipid was found to be $8.4 \mu\text{m}^2\text{s}^{-1}$ (see ESI 2.15), in good agreement with previously published calculations⁵⁸ and falls within the experimentally reported range of $5\text{-}14 \mu\text{m}^2\text{s}^{-1}$.⁵⁹ The TR-tagged lipid tail exhibited slower diffusion ($4.5 \mu\text{m}^2\text{s}^{-1}$) reflecting the hydrodynamic drag acting on the TR. During our simulations, the TR-lipids merely fluctuate slightly about their starting position. It would take a prohibitively long simulation to properly sample the diffusion of the TR-lipid over distances which could yield the formation of close interactions with LHCII, so we do not test this computationally. Instead, these simulations provide the structural model which will be used as a physically-reasonable starting point for theoretical calculations of energy transfer described below. Within the LHCII monomer, the pigment cofactors largely retain their original positions (see ESI 2.16).

Of the five TR-lipid molecules, we chose to look more closely at two in particular (labeled Tex1 and Tex2 in Fig. 5C). These were those closest to what would be the outer edge of LHCII if our monomer was part of the trimer as expected in our experimental system. We quantified the orientation of these two TR in terms of the angle between their transition dipole moment and

the normal of the membrane. One maintained an angle of $20\text{-}40^\circ$ to the membrane normal (i.e., relative to the average lipid orientation) which is consistent with earlier simulations⁶⁰ while the other adopted a nearly perpendicular orientation. We then calculated the resonance couplings between these two TR and each of the membrane-exposed Chls within LHCII (Chl $a_{610\text{-}611\text{-}612}$ and Chl b_{601} and Chl b_{608}) following the theory described in ESI 2.17. Since the distance between TR and the Chls is larger than the physical extent of the molecules themselves we assumed the point dipole approximation.⁶¹ The couplings were small, ranging from $|J| = 0.1\text{-}0.3 \text{ meV}$ for the Chl Q_y transitions and $|J| = 0.01\text{-}0.1 \text{ meV}$ for the Chl Q_x transitions, explained by the relatively large TR-Chl distances involved here (5-6 nm). For comparison, within LHCII the typical Chl-Chl separation distances are $\sim 1\text{-}2 \text{ nm}$ and the coupling ranges from 1-10 meV.

Having obtained all resonance couplings it is possible to compute first-order (Förster) rate constants for energy transfer between TR and the Q_y/Q_x states of the five Chls (see ESI 2.17). These rates also depend on the normalized spectral overlap between donor and acceptor transitions, which was calculated using an experimentally-derived TR fluorescence spectrum⁴⁴ while the Chl Q_y/Q_x transitions were assigned Gaussian lineshapes computed using a standard model of the system-bath interaction.⁶² Strictly, the acceptor states in LHCII will be a mixture of single-

molecule and excitonic states, however, since excitonic interactions in LHCII do not appear to produce significant peak-shifts or redistribution of oscillator strengths⁶² we can neglect them without qualitatively altering the calculated rates. We define the total rate as the sum of all rates associated with a single TR. Due to the relatively large distances between the randomly placed TR molecules and LHCII we obtain transfer rates of the order $k_{total}^{-1} = 6$ ns for both TR molecules considered, far longer than observed experimentally. We must therefore consider a system with shorter TR-LHCII distances in order to explain the FRET timescale observed in our spectroscopy experiments.

We then probed the distance dependence of these rates by manually moving the two chosen TR-lipids along a vector connecting the lateral position of the tagged lipid and the centre of mass of the LHCII monomer (Fig. 5D). The rates of FRET were calculated assuming a time-averaged transition dipole moment for the TR molecules (see ESI 2.18). This dependence is shown in Fig. 5E. The smallest distances assessed represent the onset of clashes between the LHCII and TR-DOPC structures. Even at these distances the calculated transfer times are > 20 ps, an order of magnitude slower than the 3.7 ps component in the TA kinetics. At these close distances the point dipole approximation will break down and couplings with Chls buried within LHCII may become significant, so our calculated transfer times are likely under-estimated. Even at these close distances, the TR chromophore lies outside of the membrane (Fig. 5D) which precludes the very close contacts needed for ~ 1 ps transfer times. However, such timescales could be achieved in theory if LHCII was closely surrounded by several TR-tagged lipids or if TR molecules relocated into the hydrophobic core of the lipid bilayer (closer to the z-position of the Chls).

3 Discussion

In this study, we generated lipid nanodiscs containing the plant LHCII antenna complex and synthetic TR chromophores and showed that they are energetically-coupled. Biochemical and steady-state absorption data determined that the assembly procedure successfully incorporated LHCII and TR into nanodiscs (Fig. 1 A-B and ESI Table S1 and S2). Steady-state and time-resolved fluorescence spectroscopy provided evidence that resonance energy transfer occurred from TR-to-LHCII with an overall efficiency of at least 60% (Fig. 1C and Fig. 2) and possibly much higher if one excludes the lipid nanodiscs not containing any LHCII. Ultra-fast time-resolved absorption data of TR-LHCII nanodiscs showed that the excited state population of TR decays on a sub-100 ps timescale with a concomitant rise of the LHCII excited state, further corroborating the high efficiency of energy transfer (Fig. 3 and Fig. 4). Computer modelling of the lipid-TR-LHCII assembly then allowed us to assess the structural dynamics and possible pathways for energy transfer (Fig. 5). The precise timescale of resonance energy transfer from TR to LHCII appeared to vary between ~ 4 ps and ~ 130 ps, depending on the continuum of possible distances between TR and LHCII that occur within the nanodisc. To provide context: a 1-10 ps timescale for TR-to-LHCII energy transfer is significantly slower than the intra-protein Chl-Chl energy transfers which are known to occur at the 100-femtosecond to single-picosecond timescale⁸ and is more compa-

rable to that of inter-protein energy transfers between neighboring LH complexes in natural thylakoid membranes.⁶³ We discuss the implications of our results below.

3.1 Molecular interpretations of experimental and theoretical data

By consideration of both our experimental ultrafast data and our computer simulations/theory we can explain the molecular nature of the TR/LHCII interaction. The nanodisc system with TR chromophores laterally diffusing around the reconstituted LHCII protein appears to have two distinct energy transfer processes: according to our TA data there is one pathway with a relatively fast 3.7 ps time constant and one pathway with a relatively slow 128 ps time constant. These are likely to relate to a subpopulation of TR which is tightly-coupled to LHCII and a sub-population of TR which appears to be more loosely coupled to LHCII. One must consider the fact that the global analysis of the TA data used to produce these time-constants finds that the best explanation is a *sequential* model for the population's time evolution (see Fig. 4B). This can be explained by the following logic: first, the pump pulse excites all TR molecules simultaneously and the first signature of the TA data, the short (3.7 ps) time constant, relates to the decay of those TR molecules which are tightly-coupled to LHCII (and the rise of excited state population for this LHCII), then, the remaining TR excited states appear as a later TA signature with a longer decay time constant (128 ps), logically, related to the subpopulation of TR molecules more loosely coupled to LHCII. Note, this subtle but important difference in the interpretation of the sequential model as a temporal evolution of a mixed population of energy donors and acceptors *rather* than being a two-step sequential transfer pathway between fixed donor/acceptor molecules which would not represent our system. We note that energy transfer rates of under 20 ps could not be achieved in our theoretical simulations with single TR molecules even at the closest TR-LHCII distances of 27 Å (see Fig. 5D). This implies that an additional TR-LHCII interaction must be taking place to bring the TR and Chl to within the 22.5 Å separation suggested by the ~ 4 ps transfer rate found in TA analysis.

We can speculate on a few possible molecular origins for the tightly-coupled population of TR. The first possibility would be a direct electrostatic attractive interaction between the TR moiety and the surface of the LHCII. This could be mediated by the negative charge of a sulfonate group which is intrinsic to the structure of TR molecule⁶⁴ interacting with amino acids protruding from LHCII, either positively-charged residues on the stromal surface, or amphiphilic helices on the luminal surface.⁷ A second possibility is that hydrophobic-hydrophobic interactions between the membrane-embedded portion of LHCII and the fatty acyl tails of the lipid attached to TR. Our MD simulations did not test for these direct interactions due to computational time limitations, but this seems feasible as lipid-protein interactions often occur between lipids and membrane proteins, including LHCII and other thylakoid proteins.^{65,66} If such attractive interactions occur then they would tend to concentrate the TR around the protein to provide a biased distribution with much shorter average TR-to-LHCII

distances than for a random distribution. If multiple TR molecules did cluster together, potentially due to one of the two interactions suggested above (or randomly), excitonic interactions between coupled chromophores would increase the rate of energy transfer to below 5 ps and explain our spectroscopy observations (due to the additive nature of transfer rates when multiple donors are interacting with a single acceptor). Note that attractive interactions between multiple TRs are quite reasonable even though TR is negatively-charged: electrostatic interactions could be mediated via positive ions (salt bridges) and/or supported by stacking between the cyclic xanthene ring of TR.⁶⁴ Another possibility is that the TR moiety does not always locate outside of the lipid bilayer but can actually flip into the hydrophobic portion of the lipid bilayer, significantly decreasing the possible TR-Chl separation and accounting for the faster than simulated rate of energy transfer.⁶⁰ Whilst this is not supported by our MD simulations which found that all TR remained outside the bilayer in various orientations, we cannot rule out the possibility of the TR entering the bilayer as other simulations of TR behaviour in lipid bilayers have suggested that this is possible.⁶⁰ The more loosely coupled population of TR represented by the 128 ps time constant in TA data is more easily explained by TR located at approximately 30–40 Å from the nearest Chl within LHCII (from inspection of the inset in Fig. 5E), suggesting a TR molecule that has a few intervening lipids between itself and the outer external surface of LHCII.

The powerful combination of experiment and theory afforded us a deeper understanding than either approach alone: experimental data guided the set-up of a realistic computer-based model which was used to assess the physical basis for energy transfers and compared directly to timescales from TA spectroscopy. This dual experiment-theory approach has proven useful in other studies of light-harvesting systems.^{13,16,67} The significance of our molecular interpretations on our TR-LHCII system is that they provide hints towards the strategic design⁶⁸ of favourable interactions between pigments and proteins which promote tight coupling and high rates of energy transfer. Specifically, we would recommend that future studies of synthetic/biological hybrid systems should look for chromophores which either promote direct attractions either between the hydrophilic external surface of the LHC protein and charged pigments or between the hydrophobic membrane subunits of LHCs and neutral pigments.

3.2 Considering the utility of nanodiscs for “enhancing” LH proteins

The procedure of forming nanodiscs appears to be successful at incorporating Texas Red into the lipid bilayer along with LHCII, as shown directly by the consistent incorporation yield (ESI Table S2) and indirectly by the fact that significant energy transfer occurs from TR to LHCII as shown by both TR quenching and LHCII enhancement of fluorescence emission (Fig. 1C, ESI Table S1). The clear benefit of the nanodisc model membrane is the “confinement” effects limiting long-distance lipid diffusion.⁶⁹ Here, the 2-D confinement of TR into a relatively small area close to LHCII has resulted in a structure where the majority of TR were

likely to be within a few nanometres distance from an LHCII protein. The enhancement of LHCII fluorescence due to TR in nanodiscs is 255% of the level for LHCII isolated within detergent micelles; our previous study of TR-LHCII proteoliposomes revealed a maximal enhancement of LHCII with a similar TR:LHCII ratio of 120%. This difference is due to the significant fluorescence self-quenching effects which are known to occur in liposomes, attributed to multiple LHCII-LHCII interactions.³⁰ Thus, if one has the goal of maximally enhancing the fluorescence of a single LH protein, our data demonstrates a clear benefit of using nanodiscs to minimize protein-protein interactions and energy-dissipative effects. Note, we are not attempting to suggest that lipid nanodiscs are always superior as a model system, merely that they are advantageous if we wish to avoid the complications of protein-protein interactions.

A disadvantage of the particular nanodisc preparation studied here was that a significant number of lipid-only nanodiscs occurred: it is likely that ~50% of the nanodiscs contained 1 LHCII along with ~40 TR and 1500 lipids and ~50% of nanodiscs contained only lipids and TR. This complicated our ensemble fluorescence measurements of TR quenching where the non-interacting population of TR led to an underestimation for FRET efficiency (see footnote §). Nonetheless, these were perfectly good samples for quantifying the fluorescence enhancement of LHCII because this measurement depends solely on the emission from LHCII, so it inherently excludes “non-LHCII” nanodiscs.⁴⁴ Furthermore, our samples were appropriate for ultrafast TA spectroscopy measurements because we were simply able to temporally distinguish between the fast-decaying TR-to-LHCII energy transfer processes separately from the population of slow-decaying TR not interacting with LHCII (~3.4 ns lifetime).³⁸

3.3 Comparison of non-covalent versus covalent strategies for interfacing chromophores and proteins

Other researchers have assessed the effectiveness of energy transfer from covalently-attached synthetic pigments to LH proteins using similar techniques as reported here; these are briefly discussed below in order to contrast to our non-covalent TR-LHCII system. Early studies demonstrated a transfer efficiency of >98% from single Rhodamine Red pigments covalently-linked to trimeric LHCII proteins, resulting in an increase of >200% in the effective absorption strength at the protein’s natural minimum absorption.³⁶ In comparison, a study using LH2 complexes from purple bacteria covalently-linked to Alexa647 pigments showed

§ The challenge for any possible purification method was that the molecular weight of these two populations were very similar (e.g. a “lipid-only nanodisc” would be comprised of ~1800 lipids (0.8 kDa each) and 6 belting proteins (22 kDa each) resulting in an ~1570 kDa final disc, whereas an “LHCII nanodisc” would comprise ~1500 lipids (0.8 kDa each), one LHCII trimer (125 kD) and 6 belting proteins (22 kDa each) forming a final ~1460 kDa disc. Size-exclusion chromatography was ineffective in our initial trials when attempting to separate these populations with similar masses. If one wished to maximize the amount of “active” TR then the population of lipid-only nanodiscs should be removed with alternative biochemical methods. This was outside of the scope of the current study because we were able to achieve our goals with the samples described.

that the attachment of multiple pigments per protein (nine /LH2) resulted in a much greater effective absorption increase, with multiple energy transfer steps occurring at time constants between \sim 0.5-20 ps leading to an overall transfer efficiency of \sim 85%, resulting in a 12-fold increase of the absorption in the natural minimal spectral region.³⁸ Reaction Center (RC) protein complexes can also be enhanced by coupling them to non-native pigments resulting increases to the photochemical activity of isolated proteins^{43,70} and to the photocurrent generated by devices,³⁹ so, approaches developed for LH antennae could be easily extended to the RC to give a photochemical output. In summary, our TR/LHCII system's demonstrated absorption enhancement of \sim 255% and transfer times of 3-120 ps is comparable to these previous reports, showing that the non-covalent strategy of introducing complementary chromophores into the lipid bilayer instead of directly crosslinking them to the protein is a viable method of artificially enhancing an LH protein's absorption cross-section. The distinct advantage offered by our self-assembly strategy is the modularity/flexibility for choosing both the pigment concentration and pigment type, without the concern for limiting factors such as a finite number of potential binding sites for attachment chemistry or genetic modification. Future studies could explore this modularity more broadly: we expect that this strategy would work for other proteins and other pigments and note that numerous synthetic pigments are commercially available (both lipid-linked and "free" pigments).

4 Conclusions

In this work we established that interfacing LH proteins to external chromophores via non-covalent self assembly can produce FRET on similar timescales to inter-protein transfer of excitation energy of the natural antenna system.⁶³ It remains to be shown whether this is due to transient chemical associations of this particular TR moiety with the periphery of the LHCII protein scaffold (electrostatic or otherwise), but we can speculate that some kind of nonspecific attractive interaction is taking place. We have demonstrated that lipid nanodiscs are ideal for the study of isolated single membrane proteins and promoting lipid-protein interactions⁷¹ and minimizing any protein-protein interactions which may distort the dynamics. In future, other small-molecule organic compounds could be incorporated into the lipid bilayer as alternative chromophores to TR, such as molecules expected to have favorable chemical associations to the protein or those with favorable spectral characteristics or interesting photophysical properties. For example, small hydrophobic molecules such as chlorins or Chl mimics⁷² which will partition directly to the central hydrophobic portion of the lipid bilayer may have even faster transfer times if they align more centrally to the Chls embedded within the LHC. Pigments which absorb at other wavelengths could be used to align to the "spectral gaps" of other LH proteins (e.g. purple bacterial complexes).^{38,39,43} Finally, synthetic organic compounds developed by the "artificial photosynthesis" community such as molecular dyads and triads^{73,74} could be added to the membrane and may couple to LH proteins in a manner analogous to what we have demonstrated possible with external chromophores in this study. Our group recently de-

veloped "hybrid photosynthetic membranes" that are comprised of natural thylakoids merged with supported lipid bilayers into microarray patterns; these have the distinct advantage of being amenable to high-resolution microscopy.^{75,76} These model membrane systems have significance as idealized platforms to test the photophysics interactions between complementary chromophores and membrane proteins relevant to both natural LHCs and artificial photosynthesis.

Conflicts of interest

There are no conflicts of interest to declare.

Acknowledgements

A.M.H. acknowledges D. Batchelor (School of Physics and Astronomy, University of Leeds, UK) for acquiring TEM data used to produce ESI Fig. S4 and D. Kohl (Faculty of Biological Sciences, University of Leeds, UK) for assistance with nanodisc belt-ing protein production. T.W acknowledges support from The Alan Turing Institute and the Chinese Scholarship Council. C.D.P.D. acknowledges support from BBSRC (grant ref: BB/T000023/1). M.S., M.N. and G.S.S.-C. acknowledge the support from the U.S. Department of Energy, Office of Science, Office of Basic Energy Sciences, Division of Chemical Sciences, Geosciences, and Bio-sciences under Award # DE-SC0018097 to G.S.S.-C.

Notes and references

- R. E. Blankenship, *Molecular Mechanisms of Photosynthesis*, 2nd Ed., John Wiley & Sons, 2014.
- G. D. Scholes, G. R. Fleming, A. Olaya-Castro and R. van Grondelle, *Nat. Chem.*, 2011, **3**, 763–774.
- T. Mirkovic, E. E. Ostroumov, J. M. Anna, R. van Grondelle and G. D. Scholes, *Chem. Rev.*, 2017, **117**, 249–293.
- X. Pan, P. Cao, X. Su, Z. Liu and M. Li, *Biochim. Biophys. Acta - Bioenerg.*, 2020, **1861**, 148038.
- X. Wei, X. Su, P. Cao, X. Liu, W. Chang, M. Li, X. Zhang and Z. Liu, *Nature*, 2016, **534**, 69–74.
- Z. Liu, H. Yan, K. Wang, T. Kuang, J. Zhang, L. Gui, X. An and W. Chang, *Nature*, 2004, **428**, 287–292.
- J. Standfuss, A. C. T. van Scheltinga, M. Lamborghini and W. Kühlbrandt, *EMBO J.*, 2005, **24**, 919–928.
- R. van Grondelle and V. I. Novoderezhkin, *Phys. Chem. Chem. Phys.*, 2006, **8**, 793–807.
- H. van Amerongen and R. van Grondelle, *J. Phys. Chem. B*, 2001, **105**, 604–617.
- A. Chenu and G. D. Scholes, *Annu Rev Phys Chem*, 2015, **66**, 69–96.
- P. G. Adams, C. Vasilev, C. N. Hunter and M. P. Johnson, *Biochim. Biophys. Acta BBA - Bioenerg.*, 2018, **1859**, 1075–1085.
- C. D. P. Duffy and A. V. Ruban, *J Photochem Photobiol B*, 2015, **152**, 215–226.
- N. Liguori, X. Periole, S. J. Marrink and R. Croce, *Sci. Rep.*, 2015, **5**, 15661.
- P. Jahns and A. R. Holzwarth, *Biochim. Biophys. Acta BBA - Bioenerg.*, 2012, **1817**, 182–193.

- 15 B. van Oort, L. M. Roy, P. Xu, Y. Lu, D. Karcher, R. Bock and R. Croce, *J. Phys. Chem. Lett.*, 2018, **9**, 346–352.
- 16 K. F. Fox, C. Ünlü, V. Balevičius, B. N. Ramdour, C. Kern, X. Pan, M. Li, H. van Amerongen and C. D. P. Duffy, *Biochim. Biophys. Acta BBA - Bioenerg.*, 2018, **1859**, 471–481.
- 17 H. van Amerongen and J. Chmeliov, *Biochim. Biophys. Acta BBA - Bioenerg.*, 2020, **1861**, 148119.
- 18 M. P. Johnson and E. Wientjes, *Biochim. Biophys. Acta BBA - Bioenerg.*, 2020, **1861**, 148039.
- 19 R. Agarwal, B. P. Krueger, G. D. Scholes, M. Yang, J. Yom, L. Mets and G. R. Fleming, *J. Phys. Chem. B*, 2000, **104**, 2908–2918.
- 20 K. L. Wells, P. H. Lambrev, Z. Zhang, G. Garab and H. S. Tan, *Phys. Chem. Chem. Phys.*, 2014, **16**, 11640–6.
- 21 H.-G. Duan, A. L. Stevens, P. Nalbach, M. Thorwart, V. I. Prokhorenko and R. J. D. Miller, *J. Phys. Chem. B*, 2015, **119**, 12017–12027.
- 22 J. Chmeliov, A. Gelzinis, E. Songaila, R. Augulis, C. D. P. Duffy, A. V. Ruban and L. Valkunas, *Nat. Plants*, 2016, **2**, 16045.
- 23 G. S. Schlau-Cohen, H.-Y. Yang, T. P. J. Krüger, P. Xu, M. Gwizdala, R. van Grondelle, R. Croce and W. E. Moerner, *J. Phys. Chem. Lett.*, 2015, **6**, 860–867.
- 24 M. Son, A. Pinnola, S. C. Gordon, R. Bassi and G. S. Schlau-Cohen, *Nat. Commun.*, 2020, **11**, 1295.
- 25 G. F. White, K. I. Racher, A. Lipski, F. R. Hallett and J. M. Wood, *Biochim. Biophys. Acta BBA - Biomembr.*, 2000, **1468**, 175–186.
- 26 I. Moya, M. Silvestri, O. Vallon, G. Cinque and R. Bassi, *Biochemistry*, 2001, **40**, 12552–12561.
- 27 M. Tutkus, P. Akhtar, J. Chmeliov, F. Gorfol, G. Trinkunas, P. H. Lambrev and L. Valkunas, *Langmuir*, 2018, **34**, 14410–14418.
- 28 A. Natali, J. M. Gruber, L. Dietzel, M. C. Stuart, R. van Grondelle and R. Croce, *J. Biol. Chem.*, 2016, **291**, 16730–16739.
- 29 D. Seiwert, H. Witt, S. Ritz, A. Janshoff and H. Paulsen, *Biochemistry*, 2018, **57**, 2278–2288.
- 30 E. Crisafi and A. Pandit, *Biochim. Biophys. Acta BBA -*, 2017, **1859**, 40–47.
- 31 S. Tietz, M. Leuenberger, R. Höhner, A. H. Olson, G. R. Fleming and H. Kirchhoff, *J. Biol. Chem.*, 2020, **295**, 1857–1866.
- 32 M. Son, A. Pinnola, R. Bassi and G. S. Schlau-Cohen, *Chem.*, 2019, **5**, 575–584.
- 33 I. G. Denisov and S. G. Sligar, *Chem. Rev.*, 2017, **117**, 4669–4713.
- 34 A. Pandit, N. Shirzad-Wasei, L. M. Włodarczyk, H. van Roon, E. J. Boekema, J. P. Dekker and W. J. de Grip, *Biophys. J.*, 2011, **101**, 2507–2515.
- 35 J. I. Ogren, A. L. Tong, S. C. Gordon, A. Chenu, Y. Lu, R. E. Blankenship, J. S. Cao and G. S. Schlau-Cohen, *Chem. Sci.*, 2018, **9**, 3095–3104.
- 36 K. Gundlach, M. Werwie, S. Wiegand and H. Paulsen, *Biochim. Biophys. Acta BBA - Bioenerg.*, 2009, **1787**, 1499–504.
- 37 M. A. Harris, J. Jiang, D. M. Niedzwiedzki, J. Jiao, M. Taniguchi, C. Kirmaier, P. A. Loach, D. F. Bocian, J. S. Lindsey, D. Holten and P. S. Parkes-Loach, *Photosynth Res.*, 2014, **121**, 35–48.
- 38 Y. Yoneda, T. Noji, T. Katayama, N. Mizutani, D. Komori, M. Nango, H. Miyasaka, S. Itoh, Y. Nagasawa and T. Dewa, *J. Am. Chem. Soc.*, 2015, **137**, 13121–13129.
- 39 Y. Yoneda, A. Goto, N. Takeda, H. Harada, M. Kondo, H. Miyasaka, Y. Nagasawa and T. Dewa, *J. Phys. Chem. C*, 2020, **124**, 8605–8615.
- 40 Y. Yoneda, D. Kato, M. Kondo, K. V. Nagashima, H. Miyasaka, Y. Nagasawa and T. Dewa, *Photosynth. Res.*, 2020, **143**, 115–128.
- 41 J. W. Springer, P. S. Parkes-Loach, K. R. Reddy, M. Krayer, J. Jiao, G. M. Lee, D. M. Niedzwiedzki, M. A. Harris, C. Kirmaier, D. F. Bocian, J. S. Lindsey, D. Holten and P. A. Loach, *J. Am. Chem. Soc.*, 2012, **134**, 4589–4599.
- 42 F. J. Schmitt, E. G. Maksimov, P. Hähti, J. Weißenborn, V. Jeyasangar, A. P. Razjivin, V. Z. Paschenko, T. Friedrich and G. Renger, *Biochim. Biophys. Acta BBA - Bioenerg.*, 2012, **1817**, 1461–1470.
- 43 K. J. Grayson, K. M. Faries, X. Huang, P. Qian, P. Dilbeck, E. C. Martin, A. Hitchcock, C. Vasilev, J. M. Yuen, D. M. Niedzwiedzki, G. J. Leggett, D. Holten, C. Kirmaier and C. Neil Hunter, *Nat. Commun.*, 2017, **8**, 13972.
- 44 A. M. Hancock, S. A. Meredith, S. D. Connell, L. J. C. Jeuken and P. G. Adams, *Nanoscale*, 2019, **11**, 16284–16292.
- 45 C. D. Blanchette, R. Law, W. H. Benner, J. B. Pesavento, J. A. Cappuccio, V. Walsworth, E. A. Kuhn, M. Corzett, B. A. Chromy, B. W. Segelke, M. A. Coleman, G. Bench, P. D. Hoeprich and T. A. Sulcik, *J. Lipid. Res.*, 2008, **49**, 1420–30.
- 46 H. Brismar, O. Trepte and B. Ulfhake, *J. Histochem. Cytochem.*, 1995, **43**, 699–707.
- 47 P. Akhtar, M. Dorogi, K. Pawlak, L. Kovács, A. Bóta, T. Kiss, G. Garab and P. H. Lambrev, *J. Biol. Chem.*, 2015, **290**, 4877–4886.
- 48 M. Son, A. Pinnola and G. S. Schlau-Cohen, *Biochim. Biophys. Acta BBA - Bioenerg.*, 2020, **1861**, 148115.
- 49 L. L. Shipman, T. M. Cotton, J. R. Norris and J. J. Katz, *J. Am. Chem. Soc.*, 1976, **98**, 8222–8230.
- 50 J. R. Reimers, Z.-L. Cai, R. Kobayashi, M. Rätsep, A. Freiberg and E. Krausz, *Sci. Rep.*, 2013, **3**, 2761.
- 51 Y. Shi, J.-Y. Liu and K.-L. Han, *Chem. Phys. Lett.*, 2005, **410**, 260–263.
- 52 W. P. Bricker, P. M. Shenai, A. Ghosh, Z. Liu, M. G. M. Enriquez, P. H. Lambrev, H.-S. Tan, C. S. Lo, S. Tretiak, S. Fernandez-Alberti and Y. Zhao, *Sci. Rep.*, 2015, **5**, 13625.
- 53 E. Meneghin, C. Leonardo, A. Volpati, L. Bolzonello and E. Collini, *Sci. Rep.*, 2017, **7**, 11389.
- 54 C. C. Gradišaru, R. van Grondelle and H. van Amerongen, *J. Phys. Chem. B*, 2003, **107**, 3938–3943.
- 55 R. Croce, M. G. Müller, R. Bassi and A. R. Holzwarth, *Biophys. J.*, 2001, **80**, 901–915.
- 56 W. K. K. T. Z. J. G. L. A. X. C. Liu Z., Yan H., *Nature*, 2004, **428**, 287–292.
- 57 M. A. Lomize, I. D. Pogozheva, H. Joo, H. I. Mosberg and A. L.

- Lomize, *Nucleic acids research*, 2012, **40**, D370–D376.
- 58 M. J. Akhunzada, F. D'Autilia, B. Chandramouli, N. Bhat-tacharjee, A. Catte, R. Di Renzo, F. Cardarelli and G. Bran-cato, *Sci Rep*, 2019, **9**, year.
- 59 G. Lindblom and G. Oradd, *Biochim. Biophys. Acta BBA - Biomembr.*, 2009, **1788**, 234–244.
- 60 M. J. Skaug, M. L. Longo and R. Faller, *J. Phys. Chem. B*, 2009, **113**, 8758–8766.
- 61 T. Förster, *Annal. Phys. (Leipzig)*, 1948, **2**, 55–75.
- 62 V. Balevius Jr and C. D. P. Duffy, *Photosynth. Res.*, 2020, **144**, 301–315.
- 63 M. Sener, J. Strumpfer, J. Hsin, D. Chandler, S. Scheuring, C. N. Hunter and K. Schulten, *Chemphyschem*, 2011, **12**, 518–31.
- 64 J. A. Titus, R. Haugland, S. O. Sharow and D. M. Segal, *J. Immunol. Methods*, 1982, **50**, 193–204.
- 65 V. Corradi, B. I. Sejdiu, H. Mesa-Galloso, H. Abdizadeh, S. Y. Noskov, S. J. Marrink and D. P. Tieleman, *Chem. Rev.*, 2019, **119**, 5775–5848.
- 66 Z. Liu, H. Yan, K. Wang, T. Kuang, J. Zhang, L. Gui, X. An and W. Chang, *Nature*, 2004, **428**, 287–292.
- 67 K. F. Fox, V. Balevicius, J. Chmeliov, L. Valkunas, A. V. Ruban and C. D. P. Duffy, *Phys. Chem. Chem. Phys.*, 2017, **19**, 22957–22968.
- 68 E. Musazade, R. Voloshin, N. Brady, J. Mondal, S. Atashova, S. K. Zharmukhamedov, I. Huseynova, S. Ramakrishna, M. M. Najafpour, J.-R. Shen, B. D. Bruce and S. I. Allakhverdiev, *J. Photochem. Photobiol. C*, 2018, **35**, 134–156.
- 69 I. Schachter, C. Allolio, G. Khelashvili and D. Harries, *J. Phys. Chem. B*, 2020, **124**, 7166–7175.
- 70 O. Hassan Omar, S. la Gatta, R. R. Tangorra, F. Milano, R. Ragni, A. Operamolla, R. Argazzi, C. Chiorboli, A. Agostiano, M. Trotta and G. M. Farinola, *Bioconjug Chem*, 2016, **27**, 1614–23.
- 71 J. I. Ogren, A. L. Tong, S. C. Gordon, A. Chenu, Y. Lu, R. E. Blankenship, J. Cao and G. S. Schlau-Cohen, *Chem. Sci.*, 2018, **9**, 3095–3104.
- 72 T. Sahin, M. A. Harris, P. Vairaparakash, D. M. Niedzwiedzki, V. Subramanian, A. P. Shreve, D. F. Bocian, D. Holten and J. S. Lindsey, *J. Phys. Chem. B*, 2015, **119**, 10231–43.
- 73 D. Gust, T. A. Moore and A. L. Moore, *Acc. Chem. Res.*, 2001, **34**, 40–48.
- 74 D. Gust, T. A. Moore and A. L. Moore, *Faraday Discuss.*, 2012, **155**, 9–26.
- 75 T. Yoneda, Y. Tanimoto, D. Takagi and K. Morigaki, *Langmuir*, 2020, **36**, 5863–5871.
- 76 S. A. Meredith, T. Yoneda, A. M. Hancock, S. D. Connell, S. D. Evans, K. Morigaki and P. G. Adams, *bioRxiv preprint*, 2020.